Tribology International 56 (2012) 107–120

Contents lists available at SciVerse ScienceDirect

Tribology International

journal homepage: www.elsevier.com/locate/triboint

Tribological behavior of electrodeposited Zn, Zn–Ni, Cd and Cd–Ti coatings on low carbon steel substrates

K.R. Sriraman [a], H.W. Strauss [a], S. Brahimi [a,b], R.R. Chromik [a,*], J.A. Szpunar [c], J.H. Osborne [d], S. Yue [a]

[a] Department of Mining & Materials Engineering, McGill University, Montreal, Quebec, Canada
[b] IBECA Technologies Inc., Montreal, Quebec, Canada
[c] Department of Mechanical Engineering, University of Saskatchewan, Saskatoon, Saskatchewan, Canada
[d] Inorganic Finishes & Corrosion, Boeing Research & Technology, Seattle, USA

ARTICLE INFO

Article history:
Received 28 October 2011
Received in revised form
29 May 2012
Accepted 7 June 2012
Available online 19 June 2012

Keywords:
Electrodeposited Zn–Ni, Cd, Zn coatings
In situ tribology
Transfer film
Tribofilm

ABSTRACT

The tribological behavior of electrodeposited Zn–Ni alloy coatings was investigated for its suitability to replace Zn- and Cd-based coatings. An *in situ* tribometry technique with a transparent sapphire hemisphere as a counter face on a pin on flat tribometer was utilized to examine the contribution of third bodies in friction and wear behavior. Wear mechanisms and tribo/transfer film morphology were also studied with the X-ray diffraction and electron microscopy. *In situ* tribometry and additional *ex situ* analyses revealed that Zn–Ni coatings had superior resistance to adhesive wear compared to cadmium coatings. Microhardness of Zn–Ni coatings was higher than Zn and Cd coatings. Hardness on the wear track of Zn–Ni coatings showed the formation of a strain hardened tribo layer.

1. Introduction

Electrodeposited cadmium based sacrificial coatings are being used in aerospace industries for anodic protection of high strength steel components. Stringent environmental concerns have restricted the extensive use of cadmium in aerospace industries. Among various coatings developed in the recent past as a replacement to Cd, Zn–Ni alloys are leading candidates that have sufficient corrosion resistance and improved mechanical properties compared to Cd based coatings. Electrodeposited Zn–Ni alloys have also shown properties of interest for automotive and aerospace industries, including their corrosion resistance [1–8], hardness [2,9–14] and thermal stability [11,13]. The anodic corrosion protection offered by Zn–Ni alloys makes it a suitable candidate to replace cadmium in aerospace industries [4].

High strength steel fasteners used in automotive and aerospace industries are often coated with Zn- or Cd-based coatings for anodic protection [15]. In addition to corrosion protection, it is also important for the coatings to have sufficient wear resistance to withstand the wear and abrasion during handling and torquing of the fasteners. It has been shown in the previous work that Zn–Ni coatings are harder than Zn [2,11]. Adequate wear resistance of Zn–Ni has been reported by Panagopoulos et al. [16] using an alumina pin on a Zn–Ni coated mild steel disc. In contrast, Cd, being a soft metal, has been shown to act as a solid lubricant during wear tests under extremely high loading conditions [17], but exhibited limited effectiveness in preventing wear. There have been several investigations on the tribological behavior of thin coating of cadmium over plated steel components to understand its friction and wear behavior under extreme conditions and controlled environments [17–19]. While the wear resistance of Zn–Ni and Cd have been evaluated individually in past studies, it is essential to evaluate the tribological behavior of the coatings of similar thickness under the same running conditions.

Both Zn–Ni- and Cd-based coatings have been investigated in the past [16,17,19] using conventional pin on disc or sliding cylinder experiments with any insight on the wear mechanisms inferred from *ex situ* techniques. While many textbooks present a well established theory on metallic friction and wear (*e.g.* [20,21]), no one as yet has conducted an investigation of metals by *in situ* tribometry. In the early eighties, Blau recommended the application of *in situ* methods to better understand and validate theories surrounding metallic friction and wear [22]. *In situ* tribometry is a novel technique developed to probe the interface between the contact surfaces to study the interface chemistry and role of third bodies in friction and wear behavior of coatings [23,24]. This technique has been successfully utilized in the past to understand the friction and wear characteristics, tribochemistry of transfer/tribo films in boron carbide coatings [23], diamond-like carbon coatings [24,25], MoS_2 based solid lubricant

* Corresponding author. Tel.: +1 514 398 5686; fax: +1 514 398 4492.
E-mail address: Richard.chromik@mcgill.ca (R.R. Chromik).

0301-679X/$ - see front matter © 2012 Elsevier Ltd. All rights reserved.
http://dx.doi.org/10.1016/j.triboint.2012.06.008

coatings [26], nanocrystalline diamond coatings [27], TiC–N [28] and Ti–Si–C–N [29] hard coatings.

The present work focuses on the investigation of tribological behavior of established industrial coating processes of Zn–Ni, Cd, Cd–Ti and Zn, using a pin-on-flat *in situ* tribometer. Wear mechanisms are examined with the help of indentation hardness, *ex situ* examination of wear track morphology, and the phase and composition of tribo/transfer films.

2. Experimental methodology

2.1. Coating processes

Five coatings on low carbon steel substrates were plated in the fashion described below. All coatings were deposited on 10×16 cm, 0.8 mm thick sheets of low carbon steel (SAE 1006). The nominal composition of the steel correspond to C, 0.04%; Mn, 0.264%; Si, 0.008%; S, 0.013%; P, 0.006%; Ti, Nb, V in traces. After deposition, the coated sheets were then mechanically sheared to 2.5 × 2.5 cm squares for all subsequent testing and analysis.

Boeing LHE Zn–Ni: Low hydrogen embrittling (LHE) Zn–Ni plating process developed by Boeing Research & Technology, USA was used [30]. An alkaline NaOH (135 g/l) and Na_2CO_3 (60 g/l) based plating solution with Zn (9–11 g/l) and Ni (0.8–1.2 g/l) metal concentrations in the ratio of 10–11:1 and additives was used, and plated in an industrial pilot plating tank. The pH of the plating bath was maintained between 12 and 13.5 at 20–25 °C and a plating current density of 48 mA/cm^2 was applied to obtain a coating thickness of 15–20 μm in 1 h. Substrates were aqueous degreased, abrasive grit blasted and activated in HCl before plating. Boeing LHE Zn–Ni will be referred to B-Zn–Ni henceforth in this paper.

Dipsol IZ C17+Zn–Ni: Commercially available Zn–Ni plating solution by Dipsol Inc. was used. An alkaline NaOH (135 g/l) based plating solution with Zn and Ni metal concentrations in the ratio of 10–11:1, with commercial additives was used, and plated in an industrial pilot plating tank. The pH of the plating bath was maintained at 12–13.5 at 25 °C and a plating current density of 28–30 mA/cm^2 was applied to produce a coating thickness of 15–20 μm in one hour. The substrates were grit blasted and acid pickled in HCl before plating. Dipsol IZ C17+ Zn–Ni will be referred to D-Zn–Ni henceforth in this paper.

Zn: The plating bath was acid chloride based with $ZnCl_2$ (60 g/l), KCl(250 g/l), H_3BO_3 (25 g/l) and HCl in smaller concentrations to maintain the pH of the bath to 4.5–4.8. The cathode efficiency was 95% and the temperature of the plating was held at 25 °C. Commercial additives were used and electroplating was performed on a laboratory-scale plating setup. A plating current density of 5 mA/cm^2 was used to generate a coating thickness of 15 μm in 2 h. The substrates were polished with 600 # SiC grinding paper and activated in HCl before plating.

LHE Cd: Low hydrogen embrittling Cd plating (LHE Cd) was plated in an industrial plating facility using an alkaline cyanide based plating solution with CdO (20–30 g/l), NaCN (90–135 g/l), Na_2CO_3 (0–60 g/l) and NaOH (11–30 g/l). A plating current density of 118–120 mA/cm^2 was used to generate a coating thickness of 15 μm in 5 min. Substrates were solvent degreased, grit blasted and acid pickled before plating. Plating temperature of 15–30 °C was used [31].

Cd–Ti: Alkaline cyanide based plating solution with CdO (18–35 g/l), NaCN (74–200 g/l), Na_2CO_3 (0–60 g/l), and NaOH (11–30 g/l) was used, and plated in an industrial pilot plating tank. Ti was added in small concentrations (40–100 ppm) for grain refinement and control of surface morphology. An initial strike was applied at a plating current density of 46–55 mA/cm^2 for 15 s to build-up a flash layer with sufficient adhesion and subsequently a plating current density of 16–32 mA/cm^2 was applied to generate a total coating thickness of 15 μm in 15 min. Substrates were solvent degreased, grit blasted and acid pickled before plating. Plating temperature of 15–30 °C was used [32].

2.2. Wear testing

During wear of materials, third bodies are generated between the two contact surfaces. The third bodies are generally classified into categories, namely tribo film, transfer film and wear debris. In terms of a counterface *versus* coating tribosystem, a tribo film (or a tribo layer), is mechanically or chemically modified layer at the coating surface, which may also consist of agglomerated wear debris. [33]. The transfer film is a layer of coating material adhering to the sliding counter face [25]. Wear debris is generally considered as any removed portion of the coating or counterface that is not part of the transfer film or tribo film. An *in situ* study of the transfer film that formed during the wear of passivated coatings was performed using a reciprocating pin on flat tribometer, equipped with a transparent sapphire hemisphere of 1/4″ diameter. By means of a video microscope mounted above the transparent counter face, the transfer film formation and dynamic changes throughout the test can be observed and later analyzed with the recorded video. A more detailed description of the instrument used here is found in [29] and a similar type of instrument is described elsewhere [26,27]. The *in situ* tribometry was conducted at a speed of 3 mm/s for 1800 cycles, which correspond to 13.44 m of sliding distance. Using a piezoelectric lateral force sensor, friction forces were recorded at a sampling rate of 2000 Hz. While omitting force recordings from the turn-around points (*ca.* 100 ms or 300 μm on each side), an average friction coefficient for each reciprocating cycle was calculated. The wear experiments were conducted using a stripe test procedure with an initial stripe length of 12 mm reduced by 2 mm successively at 10, 50, 100, 400, and 1000 cycles. Only passivated coatings were investigated for *in situ* studies because passivation is an established industrial process for electrodeposited Zn and Cd based coatings to prolong the life of the coating when the coating undergoes sacrificial corrosion to protect the substrate steel [15]. All the specimens were tested under a same normal load of 4 N, which did not contribute to a substrate effect except for the softer Cd coatings, even though the initial Hertzian contact stresses were different for the different materials: 0.69 GPa for Zn–Ni, 0.66 GPa for Zn and 0.45 GPa for Cd and Cd–Ti.

All industrial electroplated components are given a chromate passivation to prolong the life of the coating, when the coating is undergoing sacrificial corrosion. In order to overcome the risk of hydrogen embrittlement electroplated parts for aerospace applications are given a 24 h post plating baking treatment at 200 °C [15]. To better determine the wear resistances of Zn–Ni coatings, additional wear tests were performed to longer sliding distances. These tests were run for 1800 cycles at a higher sliding speed of 20 mm/s, which correspond to 31.6 m sliding distance compared to 13.44 m in the *in situ* tests. The Zn–Ni samples were tested for wear resistance under four conditions: (i) as-plated, (ii) with chromate passivation, (iii) as plated and baked for 24 h at 200 °C, (iv) with chromate passivation and baked. For endurance testing, *in situ* examination was not required. To minimize the cost impact and to utilize counterface with the same characteristics and composition, the same tribometer with opaque 1/4″ diameter alumina balls as the counterface was used for endurance testing. To determine the progression of wear at different cycle numbers, friction experiments were conducted as stripe tests similar to above but with modified initial sliding stripe lengths, where the initial 12 mm was reduced by 2 mm successively at 400, 800, and

1300 cycles. This procedure resulted in an overall 12 mm long wear scar with 2 mm sections (stripes) worn for 400, 800, and 1300 cycles and one 6 mm section worn for 1800 cycles.

2.3. Coating and tribo/transfer film characterization

X-ray diffraction in standard θ–2θ mode was performed on the unworn coating surfaces and wear tracks at different regions without any intentional removal of loose wear debris, using a Bruker Discover D8-2D diffractometer with Co Kα radiation. A DEKTAK contact stylus profilometer was used to determine the wear track profile area, which in turn was used to calculate the wear volume. An average of three profile measurements was taken to determine the wear track profile area. The wear tracks were observed and analyzed using a Philips field emission scanning electron microscope (FE-SEM) at 20 kV accelerating voltage. Compositional analysis of wear tracks was performed using Energy Dispersive Spectrometry (EDS). Microhardness of the Zn–Ni coatings was measured using Vickers hardness tester with 100 g load. For the softer Zn, Cd and Cd–Ti coatings lower loads of 50 g and 25 g were used to minimize the substrate effect. The average value over 10 indents was taken to report the hardness of the coatings. Microhardness testing was additionally carried out within wear tracks for Zn–Ni coatings at reduced load of 50 g.

3. Results

3.1. Coating characterization

The surface morphology of the unbaked coatings studied is presented in Fig. 1 and the X-ray diffraction results are presented in Fig. 3. B–Zn–Ni had uniformly distributed fine platelets less than 1 μm (Fig. 1a), while D–Zn–Ni had large platelets with intermittent porosity and platelet size greater than 10 μm (Fig. 1b). The X-ray diffraction pattern of the Zn–Ni coatings in Fig. 3(a) confirmed the formation of uniform single phase γ Zn–Ni (Ni_2Zn_{11}), which is a typical characteristic of Zn–15% Ni alloy [34]. All the peaks indexed in the diffraction pattern in Fig. 3(a) for both the Zn–Ni coatings were gamma Zn–Ni except for the peak (7 3 0) which also coincided with the Fe (2 1 1) peak. Both the Zn–Ni coatings had the composition of Zn–15% Ni and very similar phase identification by the X-ray diffraction. However, surface morphologies were quite different (Fig. 1(a) and (b)), which was a consequence of differences in plating process conditions namely the bath composition, additives and plating current density.

The morphology of Zn coating plated from acid chloride bath in the presence of additives and brighteners were in the form of hemispherical clusters (Fig. 1(c)), which are typical of Zn coatings [35]. The cluster size varied between 5 and 10 μm in size. The XRD of electrodeposited Zn, in Fig. 3(b) showed strong (1 0 0) and (1 0 1) reflections for Zn.

Electrodeposited Cd had a spherical hexagonal platelet type morphology (Fig. 1(d)) with hexagonal crystals clustering together to form a spherical structure of 10–15 μm in diameter. This type of morphology is a common characteristic of cadmium deposits [36,37]. The XRD of Cd and Cd–Ti deposits shown in Fig. 3(b) exhibited strong (1 0 1) and (1 0 2) prism plane reflections for Cd. The electrodeposited Cd–Ti coatings were different in morphology compared to the Cd coatings as shown in Fig. 1(e). Instead of spheroidal agglomeration of hexagonal crystals, stacking of individual platelets was observed. The Ti addition in the plating solution also resulted in the formation of Cd–Ti solid solution which resulted in this change in morphology.

The cross-sectional SEM of the Zn–Ni coatings is shown in Fig. 2. Both the Zn–Ni coatings consisted of through-thickness microcracks which are a typical of intermetallic gamma Zn–Ni. The Zn coating consisted of more uniform cross section devoid of microcracks. The cross-section of LHE Cd coating shown in Fig. 2 comprises columns made up of spheres with intermittent discontinuities. From the coating nomenclature, it could be understood that this type of intermittent discontinuities was intentionally provided in the coating owing to the plating conditions to facilitate the escape of co-evolved hydrogen. The cross section of Cd–Ti (Fig. 2) was also different from LHE Cd. The platelets were more densely packed without discontinuities. It is believed that the addition of Ti in the plating solution resulted in the formation of a Cd–Ti solid solution causing this change in morphology.

Microhardness values of as-deposited coatings are given in Fig. 4. Zn–Ni coatings possess higher hardness compared to Zn, Cd and Cd–Ti coatings. The reason behind higher hardness is attributed to the intermetallic phase γ Zn–Ni (Ni_2Zn_{11}) [11,13]. After baking, the hardness of the Zn–Ni coatings slightly increased while no significant changes in hardness were observed for other coatings. According to Alfantazi and Erb [10], the reason could be due to the formation of a more stable intermetallic γ phase, although no phase or structural changes in the coating were observed here due to baking treatment in Zn–Ni alloy. The difference in hardness between the two types of Zn–Ni could be explained by the fact that the intermetallic γ Zn–Ni had non-stoichiometric composition. The γ Zn–Ni can exist in varying compositions (10–14% of Ni) [14]. Hence the difference in the

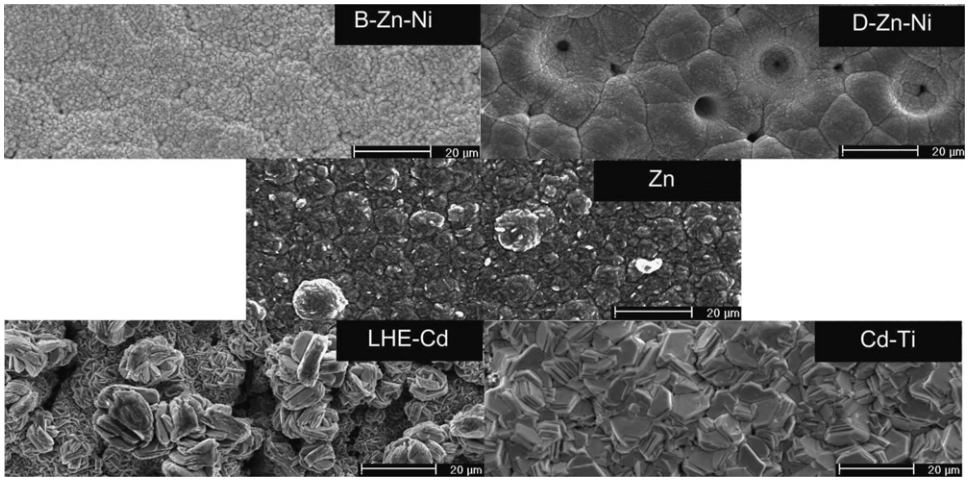

Fig. 1. Surface morphology of investigated coatings.

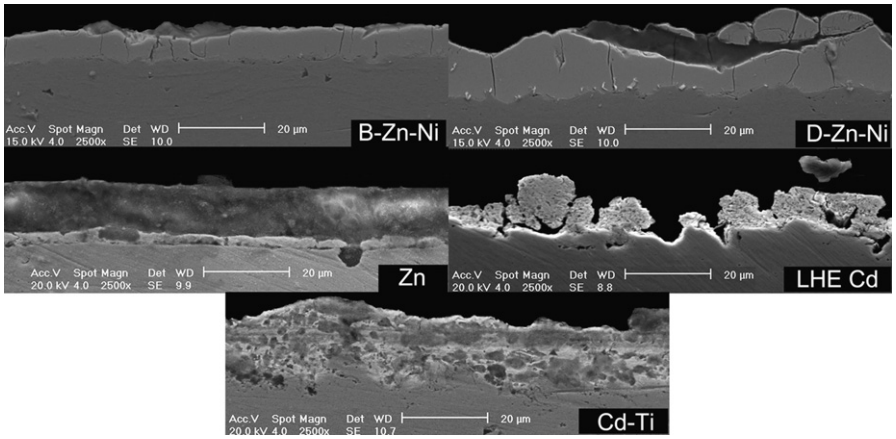

Fig. 2. SEM cross-sectional morphologies of the investigated coatings.

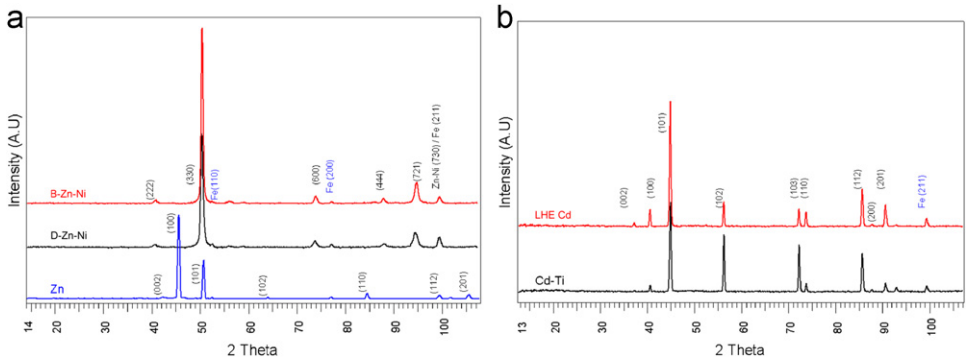

Fig. 3. XRD of investigated coatings.

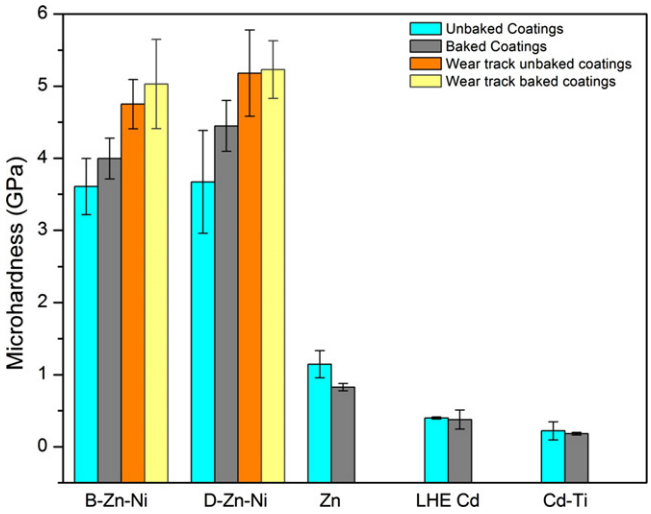

Fig. 4. Microhardness distribution of the investigated coatings.

properties could be attributed to these small differences [38]. A student '*T*' test was conducted and proved that the microhardness of the Zn–Ni coatings were statistically independent from each other.

3.2. Friction and in situ micrographs

The *in situ* micrographs obtained from the test video are shown for B-Zn–Ni in Fig. 5(a) During initial stages of wear, the initially rough coating became smooth by plowing of asperities (seen as bright spots for cycles 0 and 5). At the same time, the worn Zn–Ni adhered to the counterface, as can be seen by the rough patch appearing in the center of the micrographs for cycles 0 and 5. The size of this initial contact diameter was roughly 150–220 μm. However, as can be seen in comparing cycles 5 and 12, the adherence of the metal transfer film to the sapphire was not consistently maintained. As wear progressed, transferred material was lost and regained in various regions. In progressing toward cycle 350, the contact area grew wider, the wear track became deep enough to appear continuous and some shearing and mechanical deformation of loose wear debris was observed. At around cycle 500, the central region of transfer film was mostly removed, resulting in an occasional direct contact of sapphire on the coating surface. In progressing from cycle 500 to 600, the direct contact of sapphire on the coating became gradually more visible due to the complete removal of the transfer film within the contact regions (*i.e.* loss of transfer film stability). This led to a more compliant contact. This occurrence was accompanied by an overall increase in contact area due to lateral widening of the wear track. It is also possible that the transferred material left within the outer perimeter of the contact supported some fraction of the load. As can be seen for cycles 1000, 1400 and 1799, the optical interference fringes commonly observed for ball-on-flat contact only appear intermittently. This could be due to the roughness of the wear track, the transferred material supporting some load or a combination of both.

Friction data for B-Zn–Ni during *in situ* tests is shown in Fig. 5(b). As shown in the *in situ* images, the transfer film build-up was very rapid, where surface smoothing and transfer film formation resulted in increased contact area between metallic transfer film and the coating. This metal on metal contact exhibited friction in the range of 0.45–0.5 and was fluctuating.

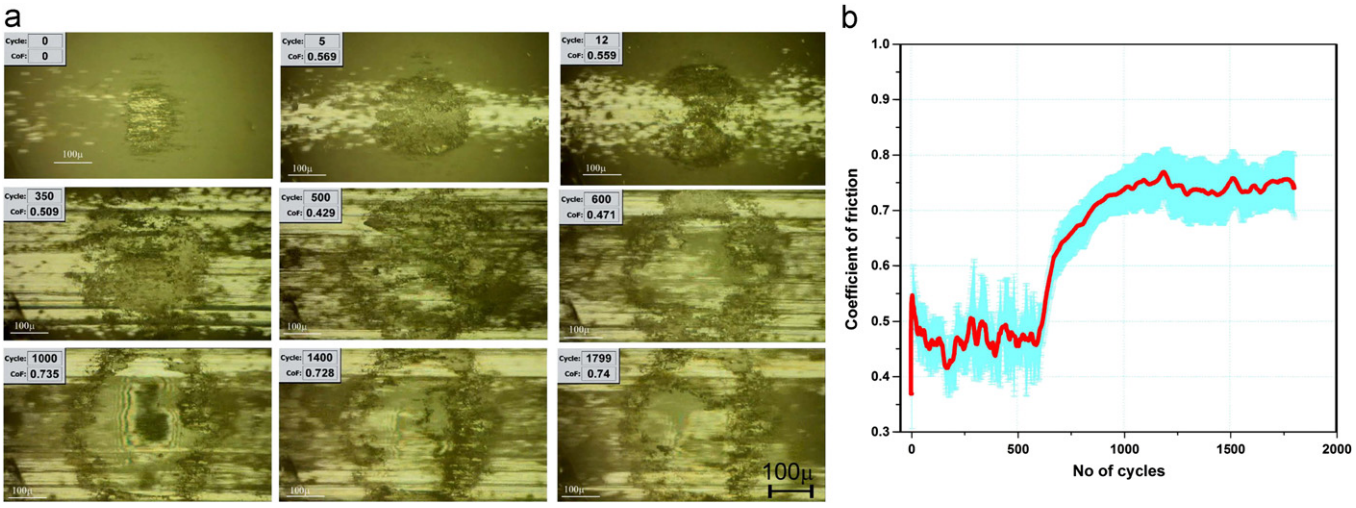

Fig. 5. (a) *In situ* micrographs for B-Zn–Ni and (b) friction coefficient *versus* No. of cycles for B-Zn–Ni.

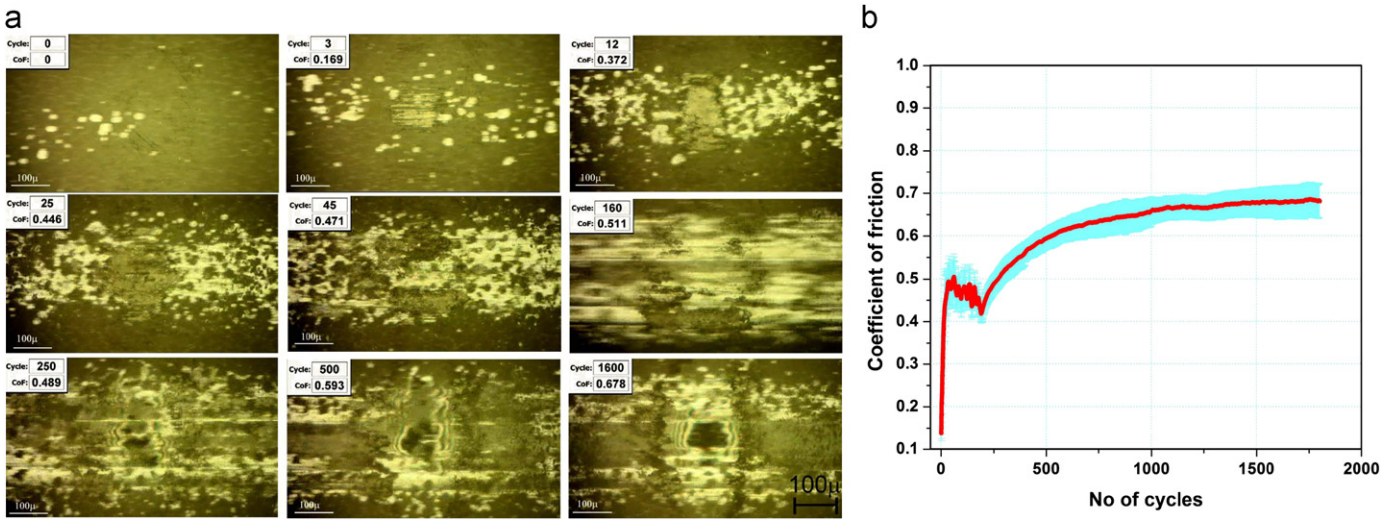

Fig. 6. (a) *In situ* micrographs for D-Zn–Ni and (b) friction coefficient *versus* No. of cycles for D-Zn–Ni.

It was also the case that the standard deviation for the friction coefficient, associated with variation in friction across the wear track, was generally high (*i.e.* 0.1). This variation in the friction across the track and from cycle-to-cycle was likely associated with the evolution of the transfer film, with material being removed and replenished in places. The fluctuations in the average friction ceased around cycle 600 and there was a stable rise in the friction coefficient from 0.5 to 0.7 until cycle 1000. This friction rise was associated with contact between sapphire and both third body debris and the hardened coating layer beneath. Beyond 1000 cycles the friction coefficient stabilized to a constant value of 0.7. During this last stage, the average friction coefficient was more stable, despite the contact appearing as intermittent between counter-face and coating.

In situ micrographs are shown for D-Zn–Ni in Fig. 6(a) The initial contact diameter was roughly 150 μm, similar to B-Zn–Ni. In the early cycle, bright spots again show the presence of ploughed asperities. The transfer film formation started more slowly than B-Zn–Ni, becoming visible around the cycle 3 and becoming continuous around cycle 12. Between cycles 12 and 25 the transfer film widened along the sliding direction, but then from cycles 25 to 45 became unstable as transfer film detachment and replenishment was observed. From cycle 45 until cycle 160, the transfer was slowly removed until sapphire on coating contact became predominant. Similar to B-Zn–Ni, the D-Zn–Ni exhibited mostly sapphire *versus* coating contact at higher cycles (see images for 250, 500, 1600 cycles), with some evidence of metal transfer film at the edges of the contact supporting some load.

During the in situ tests, the friction characteristics of D-Zn–Ni were found to be similar to B-Zn–Ni, other than a few cycles where there was a COF of 0.15 (Fig. 6(b)). Delayed transfer film build-up that was only complete around cycle 25 as opposed to cycle 2 in B-Zn–Ni showed that the initial contact of sapphire on rough coating had lower friction than transfer film *versus* wear track. For both Zn–Ni coatings, the surface smoothing during initial cycles resulted in an increase in contact area and metal-to-metal contact and consequentially higher friction. For D-Zn–Ni, friction becomes higher and starts fluctuating, which also resulted in larger deviation and changes in contact conditions. From cycle 250 onwards, after the transfer film was lost, contact of sapphire with the hardened coating was predominant, and resulted in an increase in friction coefficient.

Fig. 7(a) shows the *in situ* micrographs for electrodeposited Zn. These micrographs were obtained at a lower magnification and different lighting compared to tests previously discussed. Within the first cycle, rapid formation of transfer film occurred as can be

seen by the bright patch in the center of the images for cycle 0. The transfer film build-up continues (see cycles 2 and 30) until the coverage becomes roughly 200 μm across. As wear of the coating progresses, the wear track widens and the outer regions show limited evidence of transferred material, while the central patch remains largely unchanged (see cycle 160). However, from this point onwards (see images for cycles 180 and 200) the transfer film starts being removed until a nearly complete loss of transfer film. The bright patch in the center is now a reflection from the wear track, not a transfer film. Although not as clear for the tests on Zn–Ni coatings, the images for cycles 450, 1000 and 1799 show contact of sapphire with the coating, with intermittent appearance of optical interference fringes.

Friction coefficient *versus* cycle number is shown in Fig. 7(b) for the Zn coating. There is a very brief period at the beginning of the test where the friction coefficient is roughly 0.7, corresponding to a time when there was no transfer film and the sapphire was in contact with asperities on the coating surface. Different from the Zn–Ni coatings, this coating exhibited the highest friction (~0.8–0.85) when transfer-film-on-coating was the predominant type of contact. At about cycle 200, the friction drops to about 0.5 which was associated with sapphire-on-coating contact. From this point onwards, the friction gradually rises as the coating wears away and the contact becomes sapphire on steel substrate with some wear debris remaining in between. From separate runs, the friction coefficient of sapphire–steel contact was found to be 0.5–0.55. During the late phases in the experiment, friction only increased slightly to ~0.6, perhaps because the minimal Zn wear debris in the contact provided some solid lubrication.

Fig. 8(a) shows *in situ* micrographs for the LHE Cd coating. A very wide initial contact diameter of 400 μm was observed immediately upon sliding (see cycle 0). During the initial cycles, extensive

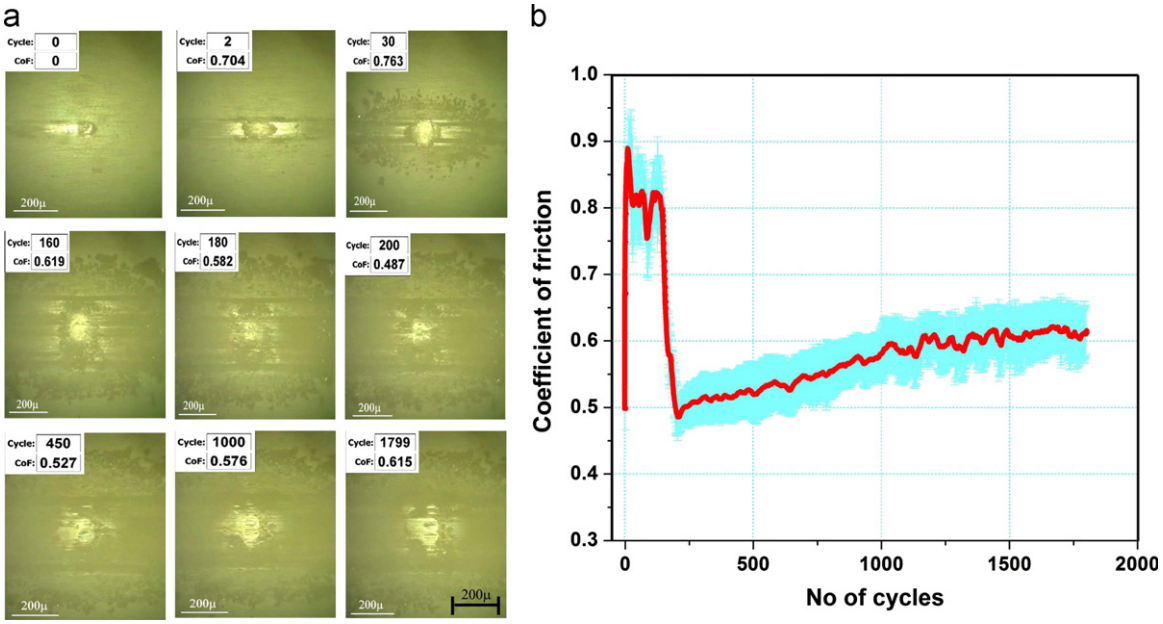

Fig. 7. (a) *In situ* micrographs for Zn and (b) friction coefficient *versus* No. of cycles for Zn.

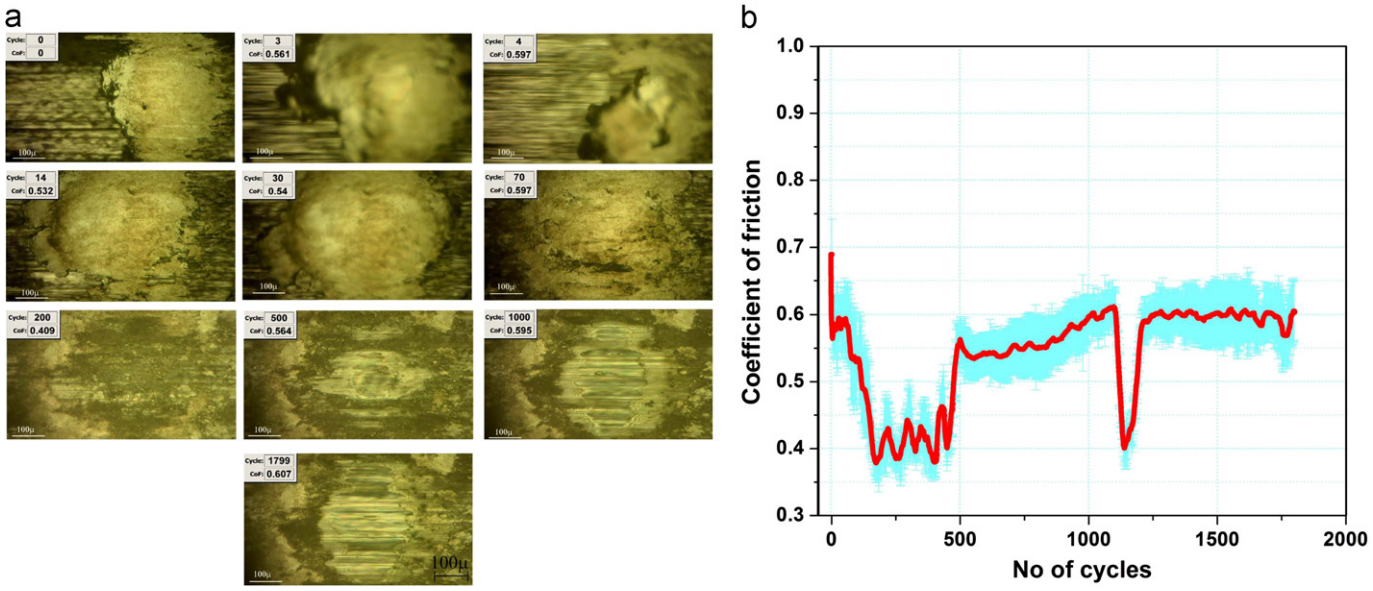

Fig. 8. (a) *In situ* micrographs for LHE Cd and (b) friction coefficient *versus* No. of cycles for LHE Cd.

transfer film formation was observed, which was thick and wide enough to completely obscure the wear track (see cycles 0 and 3). Partial loss of transfer film was observed in cycle 4, where the wear track is visible on the left-hand side. However, the transfer film was replenished by cycle 14, where the wear track was again completely obscured from view. From cycles 4 to 14, transfer film recirculation occurred, where some amount of transfer film was lost from the contact region and consequently re-accumulated again. From cycles 14 to 30 transfer film growth occurred with widening of the contact area. This was followed by transfer film detachment (see cycle 70). By cycle 200, the center of contact became visible as the transfer film was worn away and only compacted portions remained adhered (see dark patches). By cycle 500, these remaining bits of transfer film had been removed and sapphire on coating contact became apparent with intermittent appearances of the light interference patterns associated with ball on flat contact. From this point onwards, the contact area grew due mostly to coating wear. From cycle 1000 till the end of the test at 1800 cycles, mixed mode contact was observed (see images for cycles 500, 1000, and 1799). The load was primarily carried by the central sapphire on steel region while minor portion of the load was carried by transfer film on the edges of the contact area.

Friction coefficient *versus* cycle number for the LHE Cd coating is shown in Fig. 8(b). The friction coefficient starts off at 0.7 and declined to 0.4, remaining at this level but fluctuating until about cycle 500. During this time the primary type of contact was metallic transfer film *versus* the wear track. The reduction in friction occurring between cycles 1 and 250 could be related to work hardening of the transfer film and the cadmium coated surface. The variability in friction from cycles 200 to 500 appears to be related to loss and replenishment of transfer film. The following increase in friction to a level of about 0.55 was related to the formation of primarily sapphire *versus* coating contact that grew progressively for the remainder of the test. During the temporary friction drop from 0.6 to ~0.4 between cycles 1150 and 1200 (see Fig. 8(b)), *in situ* micrographs showed sporadic signs of a sapphire-on-coating contact. No other changes could be observed in the video. The explanation is that from outside the field of vision or underneath obstructed parts of the sapphire slider, a new load-carrying contact was created temporarily. The accompanying low friction coefficient of ~0.4 suggests that this contact comprised transfer-film-on-coating.

In situ video micrographs of Cd–Ti are shown in Fig. 9 (a) The wear characteristics were quite similar to that of Cd with an initial contact area of 150 μm width, observed within the first cycle. Rapid transfer film accumulation was observed again. During cycles 5–30 progressive accumulation of transfer film with partial loss and regain occurred. At cycles 40–60 the wear track width increased from 150 μm to 470 μm. At cycle 180, formation of a hole in the center of the transfer film was observed, followed by gradual widening of the hole during cycles 300 to 900. Around cycle 250, sapphire on coating contact became initially apparent. From cycles 1000 to 1800, a more compliant contact observed along with a reduction in transfer film contact diameter. A complete failure of transfer film was never observed throughout the test. After cycle 200, the contact was shared by both sapphire-on-steel in the center and the transfer-film-on-coating at the edges. However, the coating failed at 250 cycles and was consequently replaced by a tribolayer of wear debris on steel substrate. This observation was confirmed by *ex situ* SEM analysis which will be discussed in detail later.

The friction characteristic of Cd–Ti is shown in Fig. 9(b). The friction behavior of the coating was found to be increasing with accumulation of transfer film. The drop in friction coefficient at cycle 250 was due to the partial loss of transfer film. Increase in friction coefficient after 250 cycles till the end of wear test was due to mixed mode contact between the transfer film/wear debris and the steel substrate. The deviation in friction coefficient Fig. 8(b) was found to be increasing gradually from cycle 1 to 1000 cycles. Beyond 1000 cycles when sapphire on substrate steel happened to be predominant the friction coefficient as well as the deviation stabilized.

3.3. Wear results from in situ tests

The *in situ* wear data confirmed the trends observed from the friction and tribo images. A change in wear characteristic was

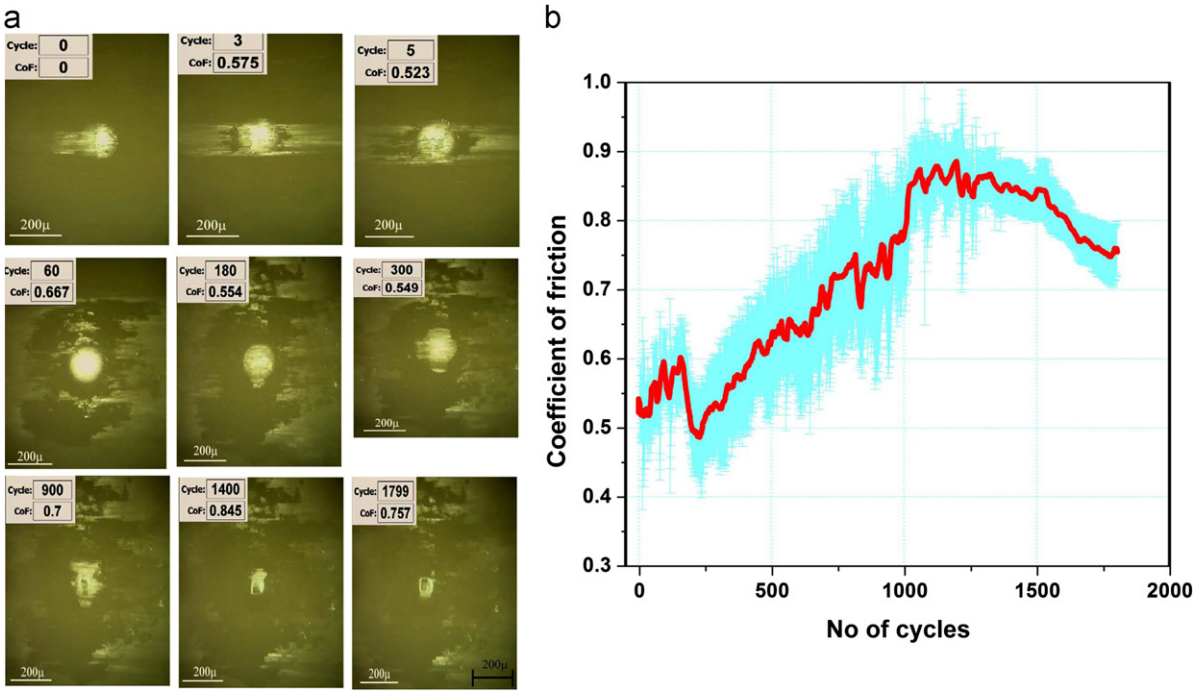

Fig. 9. (a) *In situ* micrographs for Cd–Ti and (b) friction coefficient *versus* No. of cycles for Cd–Ti.

observed with the transfer film stability. From Fig. 10(a) the wear rates for both the Zn–Ni coatings were higher due to the coating being worn until a stable transfer film was formed (till 100 cycles). The reduction in wear rate was accompanied by the shear of transfer film (600 cycles for B-Zn–Ni and 250 cycles for D-Zn–Ni) and from then on the wear rate was reduced when the sapphire on work hardened coating contact became predominant. The only difference between the B-Zn–Ni and D-Zn–Ni is the onset of transfer film separation/failure leading to formation of strain hardened coating. Fig. 10(b) shows the wear rates *versus* cycle for Zn, LHE Cd and Cd–Ti coating. They were much higher compared to Zn–Ni during the initial cycles <50, which was due to rapid transfer film formation and wear of the coating. At higher cycles (>200), the wear rate was reduced after the coating failure in Zn, which resulted in predominant sapphire on steel contact. Wear rates of LHE Cd and Cd–Ti were similar to Zn with initial higher wear rate due to rapid transfer film formation followed by drastic reduction in wear rate when contact condition changed after 250 cycles, i.e. when the coating failed leading to appearance of sapphire on steel contact (see *ex situ* wear track micrographs in Figs. 13–15). The reduction in wear rates in Zn–Ni coatings was due to formation of a strain hardened layer, which will be discussed in further sections. The reduction in wear rates after the transfer film failure in Zn was due to complete coating failure and in Cd/Cd–Ti coating it was due to partial loss of the transfer film.

3.4. Hardness measurements of tribo film

Hardness of the tribo film for Zn–Ni coatings (Fig. 4) showed considerable increase in hardness compared to the unworn coating due to strain hardening [16]. Hardness values of the tribo film could not be obtained for Zn coatings due to the absence of a consistent tribo film and also due to the removal of wear debris from the wear track during the wear tests. For Cd and Cd–Ti coatings the thickness of the tribo film was too thin for hardness measurement as sufficient spall of tribofilm was observed even for a lowest indent load of 10 gf. From the microhardness measurements on the wear track after 400 cycles it can be inferred that a strain hardened tribo film is formed on the

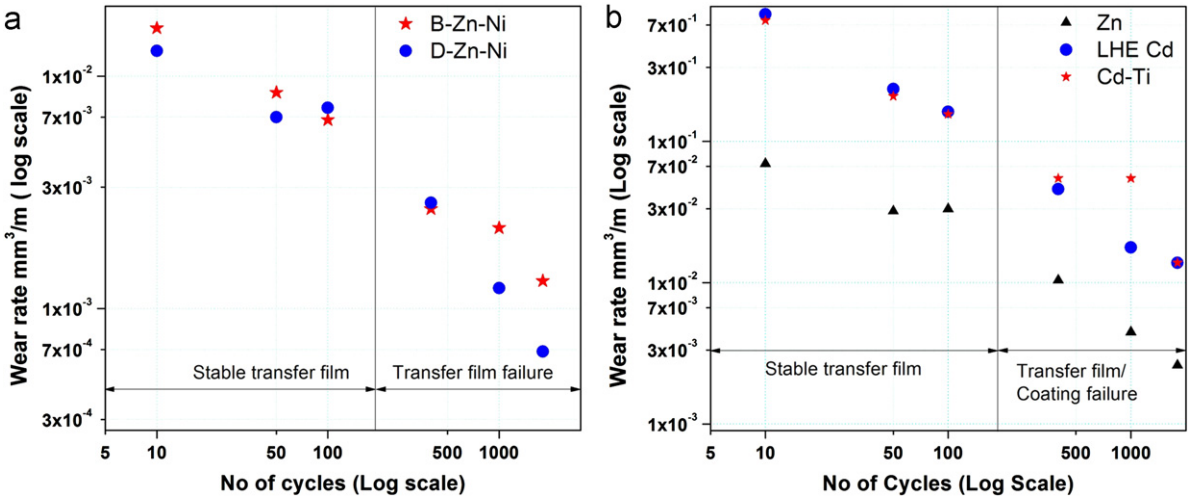

Fig. 10. Wear rates before and after transfer film failure of (a) Zn–Ni and (b) Zn, LHE Cd, Cd–Ti coatings.

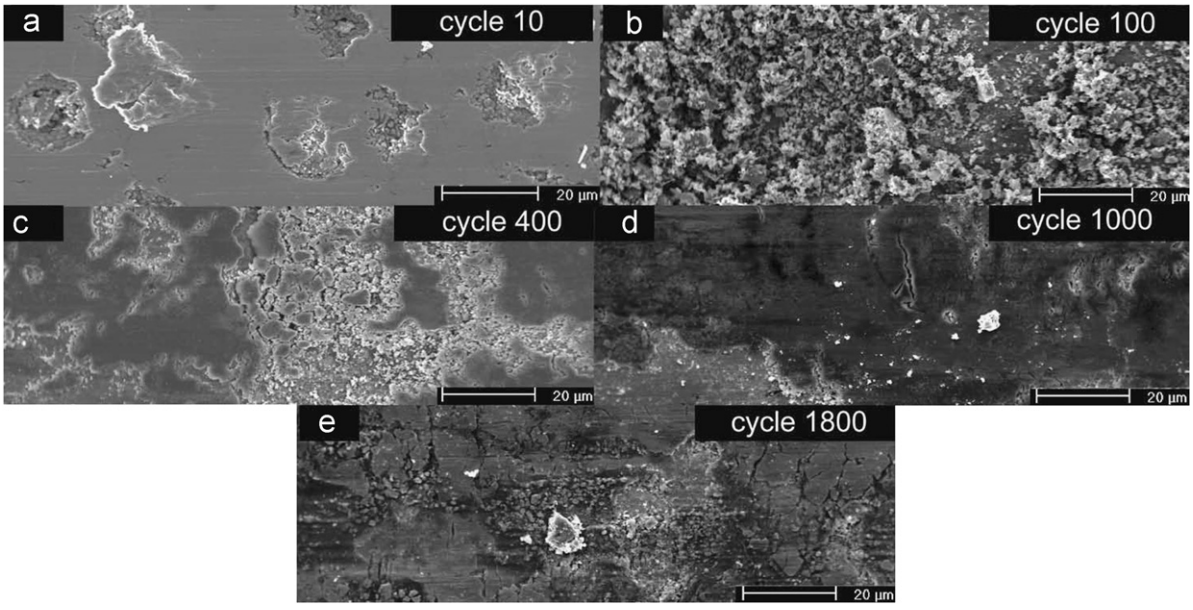

Fig. 11. Wear track morphologies of B-Zn–Ni.

Zn–Ni wear track which reduces further material removal and, as a consequence, the Zn–Ni coating lasted the entire duration of the wear test.

3.5. *Ex situ* SEM analysis of tribo/transfer film

Scanning electron microscopy performed on Zn–Ni wear tracks is shown in Figs. 11 and 12. From the *in situ* video micrographs it was shown that the nature of wear was quite similar for both the Zn–Ni coatings except for the stability of the transfer film during the wear process. The *ex situ* SEM micrographs of the wear tracks reflected similar observations. The different stages of wear were, initial smoothening of the coating surface with intermittent material removal (Figs. 11(a) and 12(a)) followed by loose wear debris accumulation (Figs. 11(b) and 12(b)). Subsequently, the loose wear debris and torn patches were entrapped in between the sapphire, transfer film and the underlying coating, forming a cracked abraded surface (Figs. 11(c) and 12(c)). This then further

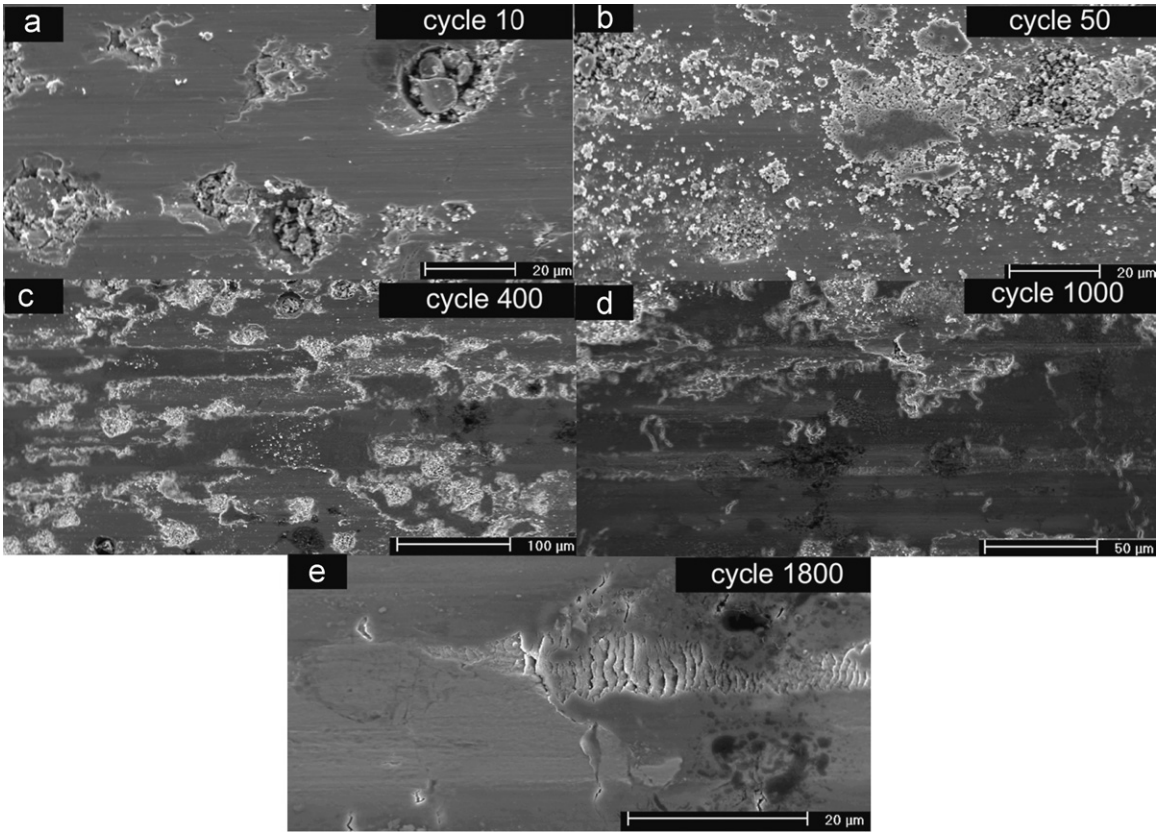

Fig. 12. Wear track morphologies of D-Zn–Ni.

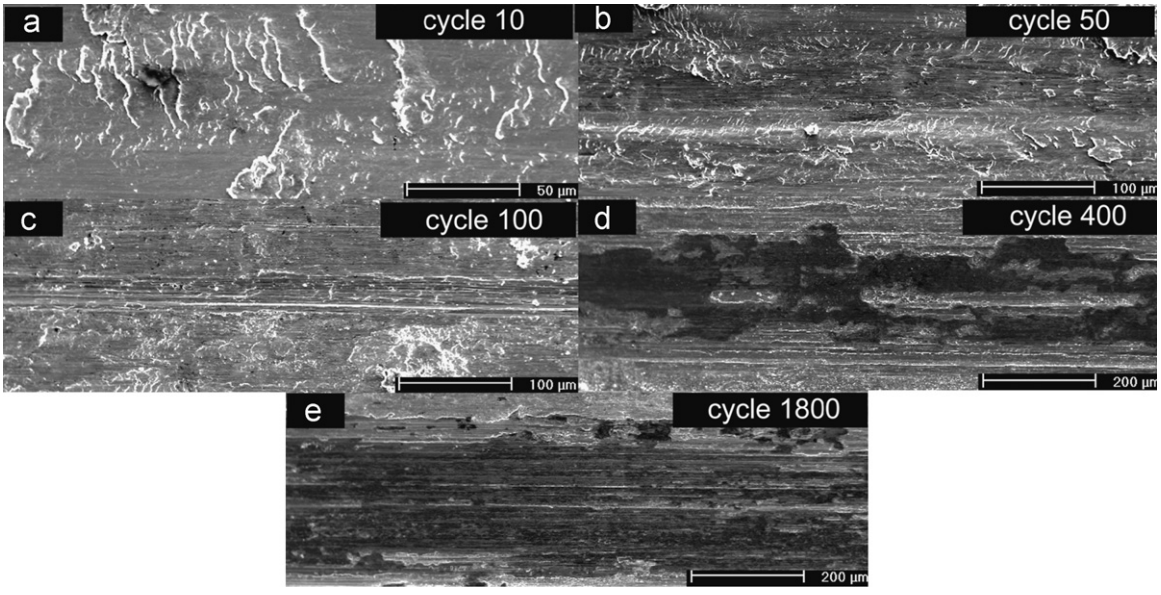

Fig. 13. Wear track morphologies of Zn.

transformed to a hardened tribolayer with transverse cracks appearing toward the end of the wear test (Figs. 11(d, e) and 12(d, e)). The difference in the onset of change of wear track morphology corresponded to the point where the transfer film lost stability. Also, it may be inferred that the morphology changes and the strain hardening of the coating occurred earlier for D-Zn–Ni at cycle 100 than at 400 cycles observed for B-Zn–Ni.

Fig. 13 shows the wear track images of Zn coating. Here the material was removed by shear and delamination (Fig. 13(a)–(b)) followed by the initiation of coating failure which resulted in contact of sapphire on steel substrate (Fig. 13(c)). As the test reached 400 cycles and beyond, the coating failed revealing torn patches of Zn coating being re-deposited during the progression of the wear test (Fig. 13(d)).

The wear track images of Cd and Cd–Ti were more similar to observations for pure Zn than for Zn–Ni. The wear track images showed initial smoothening of coating surface by extensive plastic deformation (Figs. 14(a) and 15(a)) followed by material removal by delamination (Figs. 14(b) and 15(b)). As the wear test progressed, both the coatings failed at 400 cycles (Figs. 14(c) and 15(c)) leading to the appearance of substrate steel. As the wear test progressed to further cycles, reduction in contact area of the deformed coating and widening of sapphire to steel contact was observed (Figs. 14(d) and 15(d)).

X-ray diffraction was performed on the wear tracks to investigate any phase/composition changes during wear. The results are shown in Fig. 16. The XRD of Zn–Ni wear tracks showed a stronger intensity of γ Zn–Ni peaks and a lower intensity of substrate Fe peak, while in the Cd coatings the intensity of Fe peaks were stronger than that of Zn–Ni which indirectly indicates more volume of coating material is lost during the wear of Cd coatings than Zn–Ni coatings. No evidence was found for phase changes or formation of crystalline oxides.

Ex situ analysis of transfer film formed during wear of the coatings were performed when the transfer film was stable. Wear tests were conducted on alumina sphere for 50 sliding cycles to generate the transfer film on the counterface. The transfer film micrographs are shown in Fig. 17. The transfer film accumulation/removal on the alumina ball for Zn–Ni coatings are by the process of shear and delamination of the coating surface, which is evident from the continuous layer type morphology of the transfer film (Fig. 17(a) and (b)). The Zn transfer film was found to be

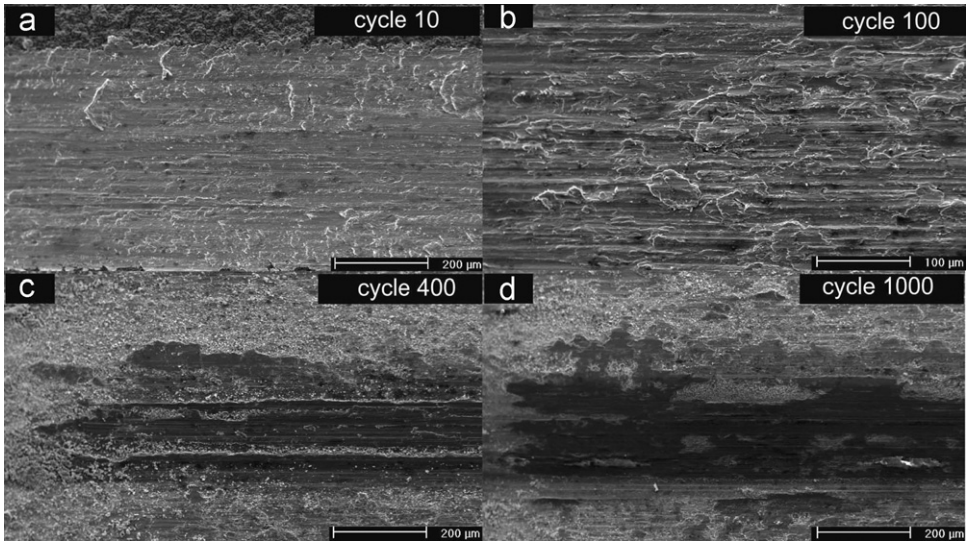

Fig. 14. Wear track images of LHE Cd.

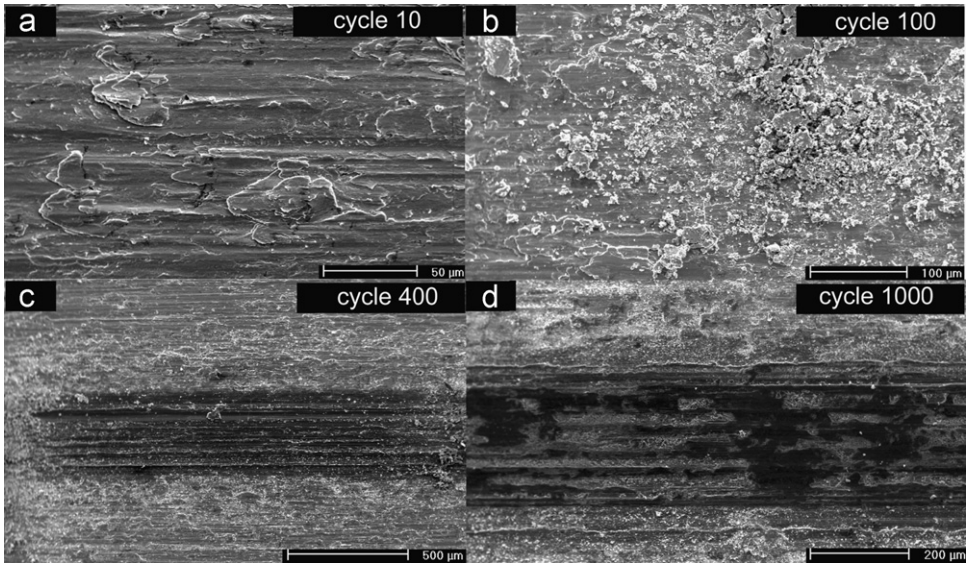

Fig. 15. Wear track images of Cd–Ti.

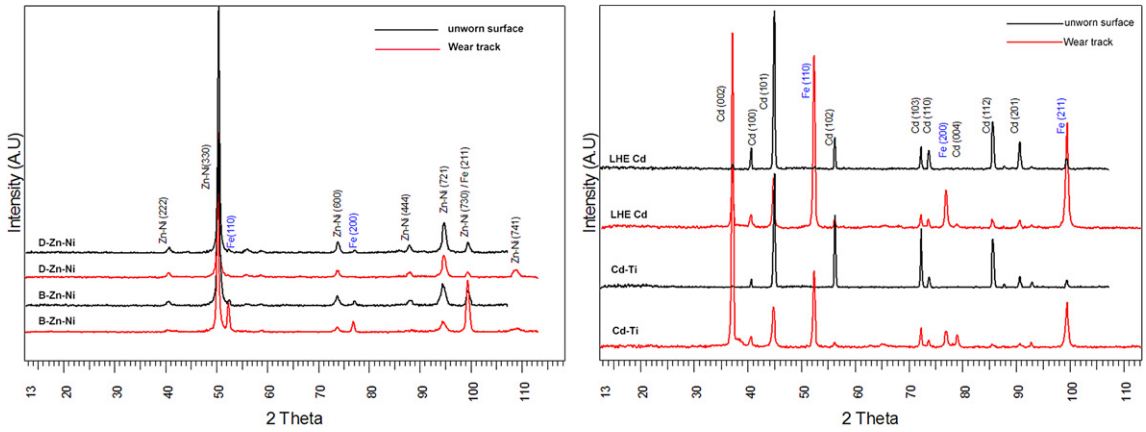

Fig. 16. XRD of wear tracks.

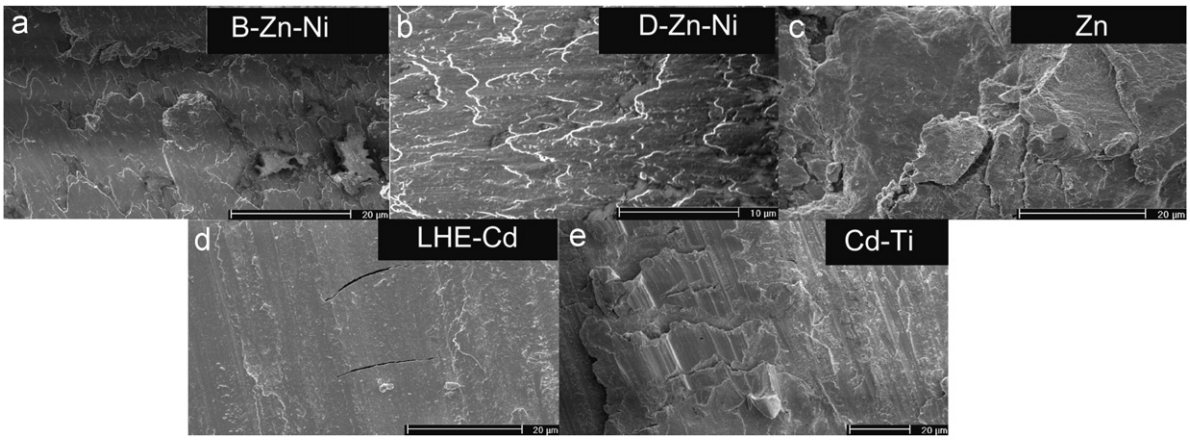

Fig. 17. SEM of transfer film formed on alumina sphere (a) B-Zn–Ni, (b) D-Zn–Ni, (C) Zn, (d) LHE Cd and (e) Cd–Ti.

composed of loose compaction of wear debris expelled from the wear track, and particle accumulation on the alumina surface (Fig. 17(c)). The transfer film formed during wear of Cd and Cd–Ti was found to be hard and adherent to alumina ball. The morphology of transfer film composed of flat facets, deformed layers and transverse cracks appearing due to the strain hardening (Fig. 17(d) and (e)).

3.6. *Longer sliding distance wear testing of Zn–Ni coatings*

From the *in situ* tests it was shown that the Zn–Ni coatings were superior to Zn and Cd coatings in terms of adhesive wear resistance. Thus, wear test on Zn–Ni coatings was performed at high speed 20 mm/s, eventually at longer sliding distance. The tests were performed for coatings with and without passivation and heat treatment. The results are shown in Fig. 18. The wear rates of Zn–Ni coatings after trivalent chrome passivation were slightly lower than the as-plated coatings. The reason behind the reduction in wear rates after passivation was due to the surface modification of the coatings by a very thin chromium oxide layer which resisted the material removal. Baking the coating also slightly improved the wear resistance of the coatings owing to increase in the hardness.

4. Discussion

This study is the first time that *in situ* tribometry has been used to examine the role of third bodies on metallic friction. The observations made here are remarkably consistent with the current understanding of the tribology of metals, which was entirely discovered by *ex situ* methods. In fact, a suggestion to utilize *in situ* tribology methods to understand friction and wear of contacting surfaces when there is a transfer of material from one surface to another was suggested by Blau in the early eighties [22]. The mechanism and properties of metal transfer during wear of two contacting surfaces, reported by different *ex situ* methods, did not totally account for the stability of the transfer films [39,40]. For all coatings studied here, there was an initial formation of a strong adherent metallic transfer film [21]. Also true for all coatings was that this transferred material was unstable in the sense that portions of the film would break away and be replenished with other third bodies, either from wear debris or materials detached directly from the coating. Eventually, the stability of the transfer film was lost entirely, which is a feature not necessarily discussed in tribology textbooks, which often portray the process of wear in metals as constantly reforming the transfer film after its stability is lost (*e.g.* [21]).

One of the utilities of using *in situ* tribology for our study of Cd and Cd-replacement coatings is that the technique provides us with precise knowledge for when the transfer films are worn away. Thus, it was determined when metal *vs.* metal friction and sapphire *vs.* metal friction was measured (see Table 1). This is important as the intention of a Cd coating on, for example a fastener, is that the coating will provide the initial lubricity to torque the component without being entirely worn away. For this application, the metal *vs.* metal friction and the wear resistance during this stage of the sliding process is most important. Table 1

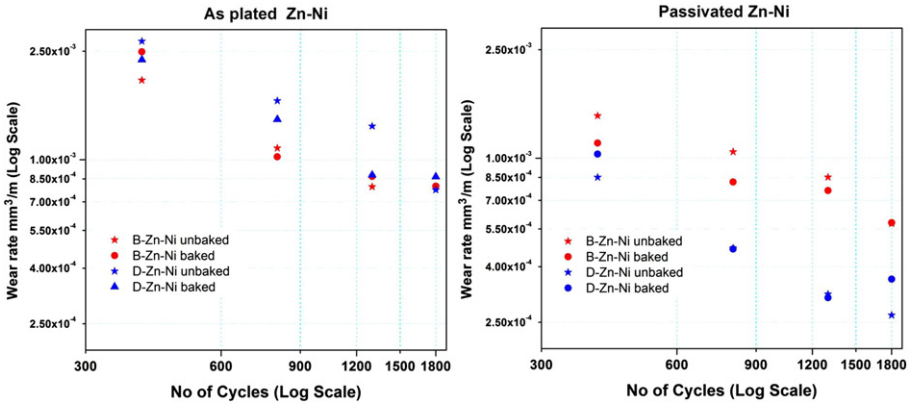

Fig. 18. Wear rates in mm^3/m of Zn–Ni coatings subjected to baking and passivation.

Table 1
Summary of *in situ* tribology test during the stage when transfer film is in contact with the coating.

	B-Zn–Ni	D-Zn–Ni	Zn	Cd	Cd–Ti
Transfer film stability (cycles)	600	200	250	500	250
Coating life (based on wear depth) cycles	1800	1800	~400	~250–300	~250–300
Wear rate $A_{300}\times10^{-3}$ (mm^3/m)	2.13	2.09	9.63	17.50	17.90
COF before TF failure	0.47–0.55	0.15–0.51	0.5–0.9	0.4–0.7	0.5–0.6
COF after TF failure	0.55–0.80	0.5–0.75	0.5–0.65	0.45–0.60	0.5–0.90
COF after coating failure	–	–	0.5–0.65	0.45–0.60	0.5–0.90

lists the comparative evaluation of Zn–Ni, Zn and Cd coatings during the wear regime when the transfer film is intact.

After initial cycles, the transfer film was removed within 500 cycles for B-Zn–Ni and 200 cycles for D-Zn–Ni, Zn, Cd and Cd–Ti. While a discontinuous patch of transfer film was observed in Zn–Ni coatings, a strongly adhering transfer film was found in Zn, and Cd coatings which indicate severe adhesive wear mechanism to be predominant in Zn and Cd coatings. While the Zn–Ni coatings transfer film failure was observed around 600 cycles and 250 cycles, both transfer film and the coating failed in Zn and Cd coatings around 250 cycles. Thus, to evaluate the wear rates comparatively when the coatings were intact, wear rates at cycle 300 were compared for all the coatings, and it was observed that both the Zn–Ni coatings exhibited wear resistance superior to the Zn and Cd coatings. From the *in situ* tribology studies, with respect to the friction coefficients, wear rates and *ex situ* wear track images, it can be concluded that the life of Zn–Ni coatings is superior to other coatings examined in this study. In other words Zn–Ni coatings lasted the full wear cycle compared to Zn and Cd. Thus, for the replacement of Zn and Cd with Zn–Ni, it becomes imperative to compare the friction and wear behavior of Zn–Ni with the above mentioned coatings till stable transfer film or life of the coatings.

One of the important parameters commonly used to evaluate the wear characteristic of metal on metal wear is the calculation of specific wear rate, which is the volume of wear per unit force. The method for calculating specific wear rate, proposed by Archard and Hirst [20,41], is based on volume of wear, which is given as follows:

$$K=\frac{Q}{S*P_n} \tag{1}$$

K is the specific wear rate (mm^3/Nm), Q is the wear volume (mm^3), S is the sliding distance (m), and P_n is the normal load (N).

The wear law proposed by Archard [41] predicts wear volume as a function of sliding distance, material hardness and applied load. The limitation of Archard's law is that it does not take into account the differing contact conditions and the role of third body in micro- and nanoscale tribology experiments. In order to evaluate the coatings in microscale and to account for the third body contribution in wear, a power law for wear was utilized which was proposed by Siniawski et al. [42]

$$A(n)=A_1*n^{\beta} \tag{2}$$

where $A(n)$ is the averaged abrasion rate over n cycles, n is the number of cycles, A_1 is the abrasion rate during the first cycle of wear and β is the time dependent constant of abrasion rate. Also

$$A(n)=\frac{V_n}{d}$$

where V_n is the averaged wear volume of n cycles and d is the sliding distance for n cycles. By fitting the averaged abrasion rate with the number of cycles A_1 and β can be determined. The parameters A_1 and β help better understanding the abrasive wear rates of different coatings.

The values of the constants A_1 and β for the coatings are listed in Table 2.

The constant β is negative which is common for metal on metal contacts [42]. The β values are more negative for Cd based coatings as compared to Zn and Zn–Ni which is also evident that Zn–Ni coatings are more resistant to adhesive wear and loss of material due to material transfer. This implies that during the

Table 2
Summary of Siniawski's model parameters and error results.

Coating	A_1 (mm^3/m)	β	% Root mean square error
B-Zn–Ni	4.4×10^{-2}	−0.43	0.769
D-Zn–Ni	3.3×10^{-3}	−0.39	7.156
Zn	1.8×10^{-1}	−0.42	6.434
Cd	4.3	−0.73	0.171
Cd–Ti	3.7	−0.72	0.365

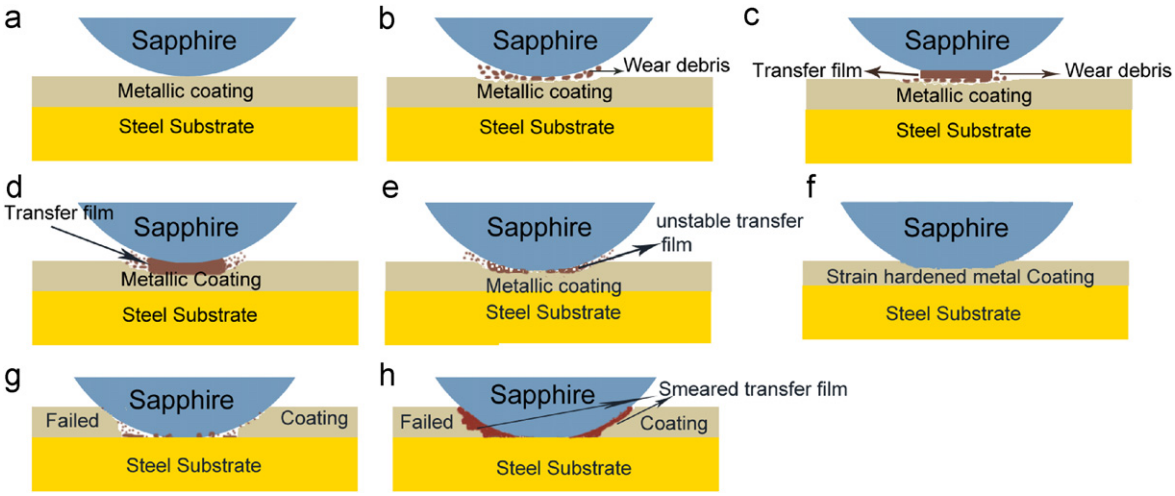

Fig. 19. Contact conditions encountered during *in situ* tribology testing of the investigated coatings.

wear regime, where the transfer film is adherent to the counterface, Zn–Ni offers maximum wear resistance due to adhesion as compared to both Zn- and Cd-based coatings.

The different contact conditions observed during *in situ* tribology studies are described in Fig. 19, starting with Fig. 19(a) showing the initial sapphire on coating contact. As the wear test progresses wear debris is generated and a contact is established between the sapphire, wear debris and the coating as shown in Fig. 19(b). Fig. 19(c) describes the transfer film formation from the wear debris and detachment from the coating. Fig. 19(d) describes the intimate contact of a stable transfer film on sapphire with the metal coating. As the wear test progresses, detachment of material from the transfer film takes place leading to an unstable transfer film as observed in Fig. 19(e). After the transfer film is totally detached or after complete failure of transfer film, the sapphire is in complete contact with the strain hardened coating as depicted in Fig. 19(f). For both the Zn–Ni coatings, the above-described model seemed to be valid until Fig. 19(f). During the progression of wear, transfer film was generated and it was the major third body contact before losing its stability. The transfer film eventually failed or detached from the sapphire, leading to intimate contact between the sapphire and the strain hardened coating, resulting in lower wear rates and increase in friction after transfer film removal.

In the case of Zn, the different stages of wear followed the trend up to Fig. 19(g). After formation of the transfer film, the transfer film and the coating eventually failed, which led to a mixed mode of contact, *i.e.* sapphire on steel substrate and small bits and pieces of strain hardened coating and wear debris trapped in between the sapphire and the steel substrate.

In the case of LHE Cd and Cd–Ti, the wear model is valid until Fig. 19(h). The transfer film and the coating failed leading to a smeared transfer film on the coating and steel substrate as described in Fig. 19(h). The transfer film instability and the coating failure occurred at the same time interval. The presence of smeared transfer film resulting in mixed mode contact and obscuring the view during the *in situ* testing was the reason behind higher friction coefficient during the progression of wear test.

5. Conclusions

In this paper *in situ* tribometry was utilized to understand third body contributions in metallic friction and wear. The nature of transfer film formation and stability, wear debris generation and contact conditions was observed to be different for Zn–Ni, Zn and Cd coatings. The transfer film characteristics were found to influence the friction and wear behavior of metallic coatings. While taking into consideration the transfer of material, adhesion, and varied contact conditions which may lead to severe galling-type seizure during torquing of threaded fasteners, Zn–Ni coatings could act as a replacement for Cd and Zn coatings based on the following conclusions:

- *In situ* tests provided greater insight toward the wear mechanisms of the coatings. Mild adhesion and material removal by delamination was observed in Zn–Ni coatings, while adhesion and large material removal in form of debris was observed in Zn coatings. Rapid transfer film formation and severe adhesive nature of wear was found to be a predominant wear mechanism in Cd and Cd–Ti coatings.
- Zn–Ni coatings showed lowest wear rates when compared to Zn, Cd and Cd–Ti coatings. Wear rates of passivated Zn–Ni coatings were found to be lower than the as plated coatings, and resistance to wear improved in Zn–Ni coatings when given a post baking treatment.
- Microhardness of Zn–Ni coatings was higher than Zn, Cd and Cd–Ti coatings. A marginal increase in hardness was observed in Zn–Ni coatings as a result of baking while no significant changes were observed on other coatings.
- No phase change was observed during wear of coatings other than mild oxidation accompanying the wear process.
- Under unlubricated conditions friction coefficient of Zn–Ni coatings were found to decrease, stabilize to a constant value and then increase after the initial run-in period. Friction coefficients of Zn–Ni were comparable to Cd coatings during the initial run in period of 500 cycles, which is beneficial when considering Zn–Ni as a replacement for Cd.

References

[1] Lambert MR, Hart RG, Townsend HE Corrosion mechanism of Zn–Ni alloy electrodeposited coatings. In: Proceedings of the society of automotive engineers. SAE, Dearborn, MI, USA; 1983. p. 81–7.
[2] Felloni L, Fratesi R, Quadrini E, Roventi G. Electrodeposition of zinc–nickel alloys from chloride solution. Journal of Applied Electrochemistry 1987;17:574–82.

[3] Fedrizzi L, Ciaghi L, Bonora PL, Fratesi R, Roventi G. Corrosion behaviour of electrogalvanized steel in sodium chloride and ammonium sulphate solutions; a study by E.I.S. Journal of Applied Electrochemistry 1992;22:247–54.
[4] Wilcox GD, Gabe DR. Electrodeposited zinc alloy coatings. Corrosion Science. 1993;35:1251–8.
[5] Alfantazi AM, Erb U. Corrosion properties of pulse-plated zinc–nickel alloy coatings. Corrosion 1996;52:880–8.
[6] Fabri Miranda FJ. Corrosion behavior of zinc–nickel alloy electrodeposited coatings. Corrosion 1999;55:732–42.
[7] Rahsepar M, Bahrololoom ME. Corrosion study of Ni/Zn compositionally modulated multilayer coatings using electrochemical impedance spectroscopy. Corrosion Science 2009;51:2537–43.
[8] Park H, Szpunar JA. The role of texture and morphology in optimizing the corrosion resistance of zinc-based electrogalvanized coatings. Corrosion Science 1998;40:525–45.
[9] Rajagopalan SR. Electrodeposition of nickel–zinc alloys. Metal Finishing 1972;70:52–8.
[10] Raman V, Pushpavanam M, Jayarkrishan S, Shenio BA. A bath for the deposition of bright zinc–nickel alloy. Metal Finishing 1983;81:85–90.
[11] Alfantazi AM, Erb U. Microhardness and thermal stability of pulse-plated Zn–Ni alloy coatings. Materials Science and Engineering A 1996;212:123–9.
[12] Barceló G, Sarret M, Müller C, Pregonas J. Corrosion resistance and mechanical properties of zinc electrocoatings. Electrochimica Acta 1998;43:13–20.
[13] Bories C, Bonino JP, Rousset A. Structure and thermal stability of zinc–nickel electrodeposits. Journal of Applied Electrochemistry 1999;29:1045–51.
[14] Bruet H, Bonino JP, Rousset A, Chauveau ME. Structure of zinc–nickel alloyelectrodeposits. Journal of Materials Science 1999;34:881–6.
[15] ASTM. 2006 F1941-00 Standard specification for electrodeposited coatings on threaded fasteners (Unified Inch Screw Threads (UN/UNR)). ASTM International, West Conshohocken, PA, 19428-2959, DOI: 10.1520/F1941-07 〈www.astm.org〉.
[16] Panagopoulos CN, Georgarakis KG, Agathocleous PE. Sliding wear behaviour of zinc–nickel alloy electrodeposits. Tribology International 2003;36:619–23.
[17] Ruggeri O, Sambogna G, Balboni CP, Volpato GA. Dry lubrication with soft metals: the tribological behaviour of a thin film of cadmium rubbing on carbon steel. Wear 1980;59:433–46.
[18] Jahanmir S, Abrahamson Ii EP, Suh NP. Sliding wear resistance of metallic coated surfaces. Wear 1976;40:75–84.
[19] Jahanmir S, Suh NP, Abrahamson Ii EP. The delamination theory of wear and the wear of a composite surface. Wear 1975;32:33–49.
[20] Rabinowicz E. Friction and wear of materials. New York: John Wiley; 1964.
[21] Stachowiak G, Batchelor AW. Engineering tribology. 3 ednButterworth Heinemann; 2006.
[22] Blau PJ. Mechanisms for transitional friction and wear behavior of sliding metals. Wear 1981;72:55–66.
[23] Dvorak SD, Wahl KJ, Singer IL. Friction behavior of boric acid and annealed boron carbide coatings studied by *in situ* Raman tribometry. Tribology Transactions 2002;45:354–62.
[24] Scharf TW, Singer IL. Role of third bodies in friction behavior of diamond-like nanocomposite coatings studied by *in situ* tribometry. Tribology Transactions 2002;45:363–71.
[25] Scharf TW, Singer IL. Monitoring transfer films and friction instabilities with *in situ* Raman tribometry. Tribology Letters 2003;14:3–8.
[26] Chromik RR, Baker CC, Voevodin AA, Wahl KJ. *In situ* tribometry of solid lubricant nanocomposite coatings. Wear 2007;262:1239–52.
[27] Chromik RR, Winfrey AL, Lüning J, Nemanich RJ, Wahl KJ. Run-in behavior of nanocrystalline diamond coatings studied by *in situ* tribometry. Wear 2008;265:477–89.
[28] Rebelo de Figueiredo M, Muratore C, Franz R, Chromik R, Wahl K, Voevodin A, et al. *In situ* studies of $TiC_{1-x}N_x$ hard coating tribology. Tribology Letters 2010;40:365–73.
[29] Strauss HW, Chromik RR, Hassani S, Klemberg-Sapieha JE. *In situ* tribology of nanocomposite Ti–Si–C–H coatings prepared by PE-CVD. Wear 2011;272:133–48.
[30] Tran LM, Matthias PM, Jones JH Low hydrogen embrittlement zinc/nickel plating for high strength steels. US Patent 8048285 ed.; November 1, 2011.
[31] MIL-STD-870C. U.S. Military Standard (USAF) on cadmium plating, low embrittlement, electrodeposition. Department of Defence Standard Practice; April 27, 2009.
[32] MIL-STD-1500C. U.S. Military Standard (USAF) on cadmium-titanium plating, low embrittlement, electrodeposition. Department of Defence Standard Practice; March 1, 2007.
[33] Khurshudov AG, Olsson M, Kato K. Tribology of unlubricated sliding contact of ceramic materials and amorphous carbon. Wear 1997;205:101–11.
[34] Bruet-Hotellaz, Bonino JP, Rousset A, Marolleau, Chauveau E. Structure of zinc–nickel alloyelectrodeposits. Journal of Materials Science 1999;34:881–6.
[35] Morón LE, Méndez A, Castañeda F, Flores JG, Ortiz-Frade L, Meas Y, et al. Electrodeposition and corrosion behavior of Zn coatings formed using as brighteners arene additives of different structure. Surface and Coatings Technology 2011;205:4985–92.
[36] Abd El-Halim AM, Baghlaf AO, Sobahi MI. Effect of some addition agents on the electrodeposition of cadmium from acidic chloride baths. Surface Technology 1984;22:129–42.
[37] El-Halim AMA, Sobahi MI. Effect of bath constituents and some plating variables on the electrodeposition of cadmium from acidic chloride baths. Surface Technology 1983;19:45–57.
[38] Brooks I, Erb U. Hardness of electrodeposited microcrystalline and nanocrystalline [gamma]-phase Zn–Ni alloys. Scripta Materialia 2001;44:853–8.
[39] Chen LH, Rigney DA. Transfer during unlubricated sliding wear of selected metal systems. Wear 1985;105:47–61.
[40] Heilmann P, Don J, Sun TC, Rigney DA, Glaeser WA. Sliding wear and transfer. Wear 1983;91:171–90.
[41] Archard JF, Hirst W. The wear of metals under unlubricated conditions. Proceedings of the Royal Society of London, Series A: Mathematical and Physical Sciences 1956;236:397–410.
[42] Siniawski MT, Harris SJ, Wang Q. A universal wear law for abrasion. Wear 2007;262:883–8.